Retention mechanisms of microplastics in soil environments during saturation-desaturation cycles: Impact of hydrophobicity and pore geometry

Ahmed Elrahmani, Riyadh I. Al-Raoush, Jamal A. Hannun, Mhd. Taisir Albaba, Thomas D. Seers

Science of the Total Environment 974 (2025) 179238

Contents lists available at ScienceDirect

Science of the Total Environment

journal homepage: www.elsevier.com/locate/scitotenv

Retention mechanisms of microplastics in soil environments during saturation-desaturation cycles: Impact of hydrophobicity and pore geometry

Ahmed Elrahmani [a], Riyadh I. Al-Raoush [a,*], Jamal A. Hannun [a], Mhd. Taisir Albaba [a], Thomas D. Seers [b]

[a] Department of Civil and Environmental Engineering, Qatar University, Doha, Qatar
[b] Department of Petroleum Engineering, Texas A&M University at Qatar, Doha, Qatar

HIGHLIGHTS

- Investigates effects of MPs hydrophobicity and pore geometry on retention
- Simulates retention using microfluidic experiments during flow cycles
- Hydrophilic MPs retain up to 25 % through clustering and sieving in small throats.
- Hydrophobic MPs retain up to 40 % by attaching to interfaces in high-connectivity pores.
- Mixed MPs retain up to 50 % with combined behaviors in larger surface area geometrie

GRAPHICAL ABSTRACT

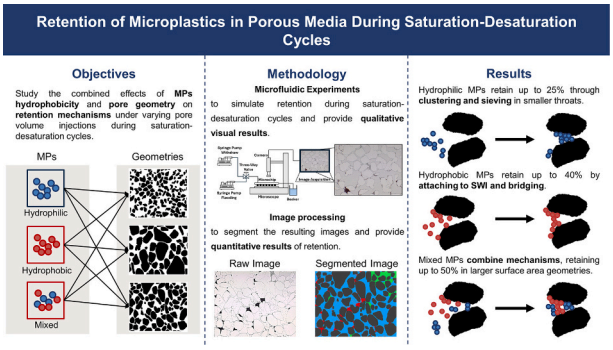

ARTICLE INFO

Editor: Susanne Brander

Keywords:
Microplastics
Porous media
Hydrophobicity
Retention mechanisms
Interface attachment

ABSTRACT

Forming ubiquitous contaminants in sediments, microplastics (MPs) are of growing concern due to their rapid infiltration into the environment and detrimental effects on ecosystems and human health. Understanding MP transport dynamics in pore networks is essential for predicting their mobility in sediments and soils and developing strategies to mitigate their spread. This study examines how pore geometry and MP hydrophobicity affect retention mechanisms within porous media during saturation-desaturation cycles. Microfluidic experiments were conducted using micromodels representing porous media with varied pore characteristics. MPs with hydrophilic, hydrophobic, and mixed hydrophobicity properties were introduced into these micromodels, and high-resolution imaging analyzed their retention patterns. The results reveal distinct retention behaviors based on MP hydrophobicity and pore geometry. Hydrophilic MPs were retained through clustering and sieving within smaller throats, particularly in low-connectivity geometries, with retention reaching 25 %. Hydrophobic MPs attached strongly to the solid-water interface (SWI) during saturation and shifted to the air-water interface (AWI) during desaturation, achieving retention rates up to 40 % in high-connectivity geometries. Mixed MPs exhibited combined behaviors, with early SWI attachment and subsequent clustering and sieving, resulting in retention rates as high as 50 % in geometries with high specific surface areas. These findings highlight the role of pore

* Corresponding author.
E-mail address: riyadh@qu.edu.qa (R.I. Al-Raoush).

https://doi.org/10.1016/j.scitotenv.2025.179238
Received 15 December 2024; Received in revised form 12 February 2025; Accepted 24 March 2025
Available online 27 March 2025

geometry and MP surface properties in determining retention and mobility. Hydrophilic MPs form contamination hotspots in fine-grained sediments, while hydrophobic MPs are more mobile in high-connectivity environments. Mixed MPs persist due to multiple retention mechanisms, posing challenges for remediation. This study informs strategies to manage MP contamination in subsurface environments.

1. Introduction

The suffusion of plastic particulate into the natural environment is of growing concern, with the microplastics (MPs) fraction (1–5000 μm ⌀) being especially deleterious due to its bioavailability and propensity to evade detection and removal from natural systems (Guo et al., 2020; Qi et al., 2020; Li et al., 2021; Yang et al., 2021). Detrital MPs exhibit diverse geometries, compositions, and surficial properties, arising from both the inherited characteristics of their proto-polymers, and physicochemical alteration by diagenetic processes, such as photothermal degradation, biodegradation, and mechanical wear (Gola et al., 2021; Li et al., 2021). The broad global distribution of MPs in recent sediments, ranging from marine environments to terrestrial settings, has raised concerns about their impact on ecosystem function and the potential risks they pose to human health via transmission through the food chain (De Souza MacHado et al., 2018; Smith et al., 2018; Gola et al., 2021; Jannesarahmadi et al., 2023). MPs pollution in terrestrial environments, particularly within soils, is alarming, given the reliance of agriculture upon the pedosphere. Recent studies indicate that the abundance of MPs in terrestrial environments may surpass that of the oceans, with farmland soils receiving annual inputs that potentially exceed that incurred by the oceans by more than an order of magnitude (Horton et al., 2017; Guo et al., 2020; Qi et al., 2020). Understanding the transport dynamics of MPs within soils and sediments, particularly within the vadose zone where complex cycles of wetting and drying are encountered, is of paramount importance, given that this forms the locus of human interaction with the Earth's derma layers, and constitutes arguably the most prolific pathway for MPs contamination and mobilization in terrestrial settings (Zhang et al., 2014; Li et al., 2021; Esfandiari et al., 2022). Understanding MPs transport dynamics in multifarious pore systems under spatiotemporally evolving saturation profiles is thus critical towards understanding the migratory pathways and fates of MPs within soils and sediments, providing insights into to the degree to which such natural porous media act as a sink for MPs contaminants or a source for their transmission into coupled components from the hydrosphere and biosphere. Broadening this fundamental understanding of MPs mobility will in turn better inform efforts to mitigate their proliferation within shallow subsurface settings, particularly in the context of hydrogeology and groundwater engineering (Chen et al., 2010; Zhang et al., 2011; Song and Kovscek, 2016; Hannun et al., 2022).

The commonly held perception that MPs are hydrophobic agents has recently shifted due to insights from the literature. While inherently hydrophobic, their surfaces can readily undergo alteration when exposed to hydrophilic pollutants or surfactants (Jiang et al., 2021, 2022; Anastopoulos et al., 2022). In particular surfactant molecules can adhere to the MPs surface through van der Waals and hydrophobic forces, with the hydrophobic tail of the surfactant interacting with the non-polar structure of the MPs, exposing its hydrophilic component to its ambient surroundings, thus leading to a reduction in hydrophobicity (Xia et al., 2020). This observation is pivotal towards their transport behavior at the pore scale, especially for smaller MPs or plastic contaminants within the colloidal size range (i.e., nanoplastics: NPs), given their higher specific surface area (Sun et al., 2022). For such size fractions, understanding the behavior of plastic particulate transport in geologic porous media under two phase immiscible flow presents considerable challenges, as MPs/NPs retention and release within individual pores is strongly coupled with the given hydro-chemical conditions met therein. These complexities are pertained to the relative strength of adhesive forces and torque resistance, as well as the hydrodynamic and torques applied (Bergendahl and Grasso, 2000; Shen et al., 2007; Molnar et al., 2011; Dong et al., 2018; Liu et al., 2020; Koutnik et al., 2022; Liang et al., 2022; He et al., 2023). Among these, hydrodynamic forces emerge as a dominant factor promoting fines mobility, which can be related to increasing seepage velocity at the pore scale (Bradford et al., 2011; Zhao et al., 2019; Nishad et al., 2021; Nishad and Al-Raoush, 2021). It is worth noting that seepage velocity is not solely determined by the flow velocity. Pore-morphology (i.e., size, shape, roughness, coordination number and tortuosity), which varies significantly across different geologic porous media, plays a pivotal role in controlling the seepage velocity (Liang et al., 2013; Elrahmani et al., 2024; Jung et al., 2018). In systems characterized by large, interconnected pores, MPs may experience relatively high seepage velocities, allowing for rapid transport through the porous matrix. Conversely, in media with limited, tortuous flow paths, MPs may encounter reduced seepage velocities leading to stagnated mobility and retention within the pores (Elrahmani et al., 2023). Equally, larger size, shape or concentration of MPs increases the probability of retention within the porous media (Jung et al., 2018; Hannun et al., 2022; Elrahmani et al., 2023). Moreover, changes in solution chemistry, encompassing variations in ionic strength, pH, and ionic composition, influence the retention of MPs adhering to solid surfaces (Tong et al., 2020; Dong et al., 2022a, 2022b; Wang et al., 2022a; Xu et al., 2022). For example, MPs residing in the secondary minima of interaction energy tend to be released when the solution's ionic strength decreases, leading to the secondary minimum diminishing under low ionic strength conditions (Hahn and O'Melia, 2004). However, the situation becomes more complex when dealing with MPs in the primary minimum. The DLVO (Derjaguin, Landau, Verwey, and Overbeek) theory predicts an infinite depth of the primary minimum under favorable conditions, rendering the release of MPs from a smooth surface practically negligible (Shen et al., 2012; Torkzaban et al., 2013).

Laboratory column experiments have been used to study the transport of MPs with unfavorable attachment characteristics under variety of flow rates and solution chemistries (Bradford et al., 2011; Bradford and Kim, 2012; Liang et al., 2013; Bradford and Torkzaban, 2015; Sun et al., 2015; Torkzaban et al., 2015; Ling et al., 2022). Column experiments, while informative, have limitations, particularly in explaining anomalous observations, such as the fractional release of MPs under conditions of decreasing ionic strength, where adhesive forces are predominantly repulsive (Shen et al., 2012; Torkzaban et al., 2013). These experiments typically do not resolve fines transport phenomena at the pore-scale, including straining, resulting from baffles presented by grain contacts and small pore throats, size exclusion, ripening, bridging, clogging, and attachment to nanoscale surface heterogeneities or fluid-fluid menisci, all of which play pivotal roles in the net mobility of MPs in porous media.

Further to this, mathematical modeling has also been employed to predict MPs release behavior within porous media, though such models are often limited due to their inability to incorporate pore-scale transport mechanisms, which are crucial for accurately capturing their targeted behavior. Despite recent efforts to incorporate mechanisms such as mechanical filtration and straining in modeling frameworks (Tosco et al., 2009; Pazmino et al., 2014; Bradford and Leij, 2018; Dichgans et al., 2023), modeling approaches still tend to exhibit poor agreement with experimental data due to abstractions in their representation of MPs transport. This discrepancy underscores the critical need for experimental studies which are able to explicitly visualize pore scale MPs trapping and transfer mechanisms, which in turn can provide a

more comprehensive understanding of continuum scale MPs transport dynamics.

In view of the above, this study aims to reveal the interplay between pore geometry and MPs hydrophobicity in governing retention mechanisms within porous media during saturation-desaturation cycles. The objective is to better understand, at the pore-scale, the impact of MPs surface chemistry and pore space characteristics on the retention dynamics of MPs at key interfaces (i.e., solid-water (SWI), air-water (AWI), and air-solid (ASI) interfaces). This in turn quantifies the capacity of porous medium to act as sinks for MPs under dynamic flow conditions, providing critical insights into their retention and transport behavior. To achieve this, a series of controlled microfluidic experiments were conducted using micromodels with pore geometries fabricated to mimic natural soil systems. MPs with hydrophilic, hydrophobic, and mixed hydrophobicity properties were injected through the micromodels, and high-resolution images were acquired to capture retention patterns and quantify MPs distribution across interfaces at variable experimental conditions.

The novelty of this work lies in establishing a bottom-up framework that links MPs attachment across distinct interfaces (i.e., Air-Water, Air-Solid, and Solid-Water) with the broader retention dynamics in the flow field, offering a comprehensive perspective on MPs interactions in porous media under dynamic flow conditions. Furthermore, this study advances our understanding of retention mechanisms by capturing the combined effects of pore geometry and MPs hydrophobicity across varying pore volume injections, moving beyond traditional steady-state approaches to reveal the temporal and spatial variability of MPs retention mechanisms. Additionally, as the microfluidic imaging offers qualitative insights into pore-scale behavior, it is systematically translated into quantitative results through image processing techniques. This approach effectively bridges empirical observations with quantitative analysis, enhancing our understanding of porous media as effective MPs retention systems.

This manuscript is organized as follows: Section 2 details the physical properties of the MPs and porous media studied, along with the experimental procedures and image processing techniques employed. Section 3 presents the experimental results, including visual observations on the effects of MPs hydrophobicity and pore geometry on retention, as well as quantitative data supporting these findings. Finally, Section 4 summarizes the main conclusions drawn from this research.

2. Material and methods

2.1. Microplastics characteristics

The study employed two species of MPs obtained from Magsphere Inc. (Pasadena, CA, USA): hydrophobic Polystyrene (PS) and hydrophilic Carboxylate Modified Polystyrene (CMPS). Both have a mean diameter of 5 μm and a density of 1.05 g/cm^3. Three MPs suspensions were prepared (i.e., hydrophobic, hydrophilic, and mixed hydrophobic-hydrophilic) and each suspension was uniformly dispersed in deionized (DI) water at a concentration of 0.1 %, with a ratio of 1:1 utilized for the mixed hydrophobic-hydrophilic suspension. Each suspension was prepared by combining 100 μL of MPs stock solution with DI water to achieve a final volume of 10 mL.

The concentration of MPs in the prepared suspension was 1.46×10^7 MPs/mL, which is higher than typical values reported in natural sandy soils (O'Connor et al., 2019) or in treated wastewater (Wang et al., 2021). The concentration used in this study was selected based on findings from previous studies (Nishad et al., 2021; Nishad and Al-Raoush, 2021), which demonstrated that under controlled conditions, high MPs concentrations accelerate the clogging process, making it possible to observe retention and transport mechanisms within a practical experimental timeframe. Moreover, significantly higher concentrations have been observed in certain environments, including urban and industrial soils with up to 12,000 particles/kg (Jacques and Prosser, 2021; Koutnik et al., 2021) and agricultural soils with concentrations reaching 43,000 particles/kg due to plastic mulch and biosolid applications (Katsumi et al., 2021; Yang et al., 2021). Industrial soils have been found to contain up to 7 % MPs by weight (Wang et al., 2023), highlighting the potential for high accumulation in localized areas. Over time, surface deposition, vertical migration, and lateral transport contribute to the retention and buildup of MPs in porous media (Han et al., 2022; Li et al., 2023b). Environmental factors such as erosion, UV degradation, rainfall, and soil composition further influence MP retention (Harley-Nyang et al., 2023; Liu et al., 2024), leading to increasing concentrations in soils and sediments. It is important to note that even at lower MP concentrations, clogging can still occur, as it is not solely a function of MP concentration but also depends on particle size, pore geometry, and aggregation behavior. Research has shown that fine particle clogging occurs even at low concentrations when the pore-to-particle size ratio falls within the range of $1.67 < o/d < 100$ (Elrahmani et al., 2023, 2024). MPs can cause internal clogging by accumulating at pore throats or surface clogging when larger particles obstruct flow paths (Fang et al., 2022). Additionally, aggregation and deposition processes further contribute to permeability reduction, even in dilute MP suspensions (Li et al., 2023a; Zhou et al., 2023).

Before initiating experiments, MPs suspensions underwent one minute of sonication using an ultrasonic processor (SONICS, Vibra cell) at 20 °C to prevent the high heat of sonication from impacting the structural integrity of the MPs. Zeta potential values were measured at 20 °C using a Zetasizer (Nano ZSP, Malvern Panalytical, Southborough, MA) to establish the MPs suspension electrokinetic properties. Zeta potential measurements for the hydrophilic, hydrophobic, and mixed hydrophilic-hydrophobic suspensions were −12.756 mV, −21.622 mV, and −16.767 mV, respectively. Fig. 1 presents the computed DLVO energy profiles of MPs-MPs and the MPs-collector interactions. The collector is PDMS with Zeta potential of −60 mV.

2.2. Micromodels

Custom PDMS micromodels measuring 6.7 × 5 mm were fabricated to mimic natural porous media and used for MPs suffusion experiments. Specifically, these microfluidic devices comprised three geologically realistic pore geometries (Fig. 2) with a channel depth of 20 μm. Pore geometries were extracted from 3D images of sand packs obtained using synchrotron x-ray micro-computed tomography acquired at the Argonne National Laboratory (ANL) synchrotron facility (Al-Raoush, 2012; Jarrar et al., 2020, 2021). To prepare the microchips geometries from raw 2D ortho slices, selected tomograms were binarized via global thresholding. Grain boundaries were identified by constructing line segments with a non-zero gradient value between adjacent pixels. Following this, pore throats were reinstated and expanded using a watershed segmentation technique paired with controlled dilation. The watershed algorithm, applied to the gradient map, isolated individual pore spaces and delineated throat regions between them. Dilation then refined throat dimensions to ensure connectivity while maintaining geometric accuracy. Manual editing was used where needed to adjust critical areas, resulting in a well-defined pore network representative of natural porous media. The micromodels were fabricated using lithography utilizing polydimethylsiloxane (PDMS) to form the geometry of the chips. Comprehensive details regarding the construction of studied geometries can be found in Elrahmani et al. (2022). The properties of each pore system are summarized in Table 1.

Fig. 3 presents the probability distributions of grain size, pore size, throat size, and pore aspect ratio for the three analyzed geometries. To assess the statistical significance of the differences in pore aspect ratio values among the geometries, an ANOVA test was conducted. The ANOVA test was performed using MATLAB (R2023b) using a sample size equal to the number of pores identified in each geometry, which ranged from approximately 50 to 100 depending on the pore structure. Prior to the analysis, data normality and homogeneity of variances were

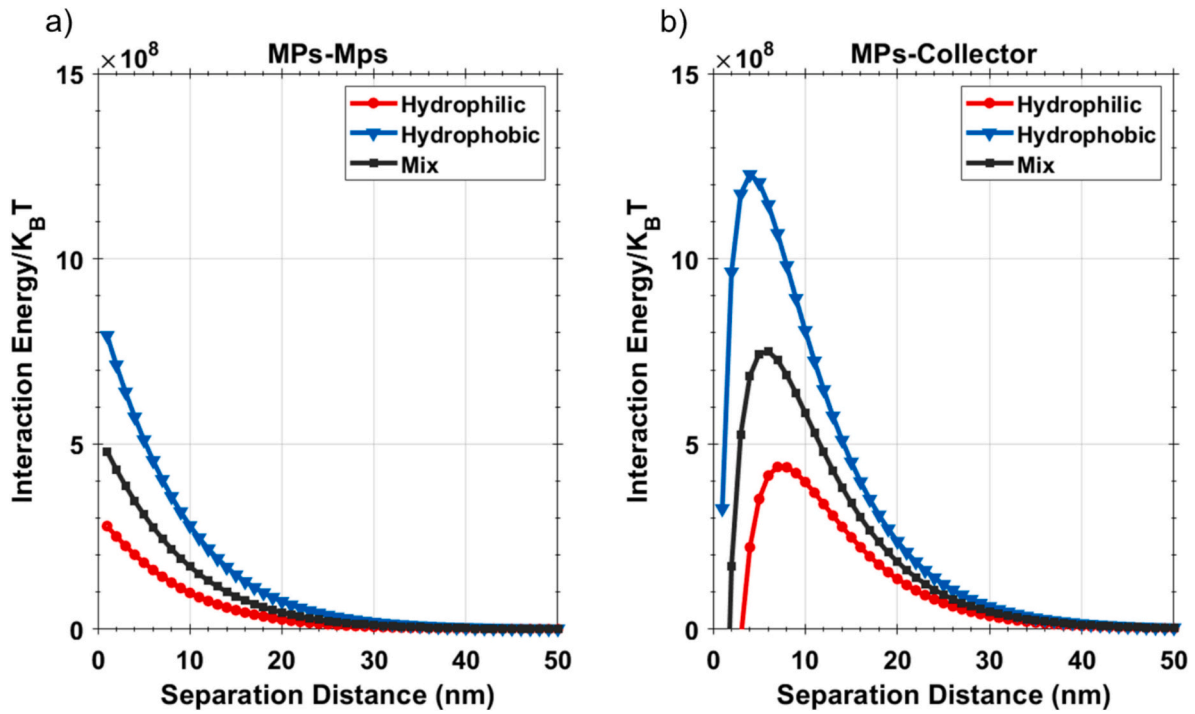

Fig. 1. DLVO energy profiles for various microplastics interacting with; (a) other microplastics, and (b) the collector surface.

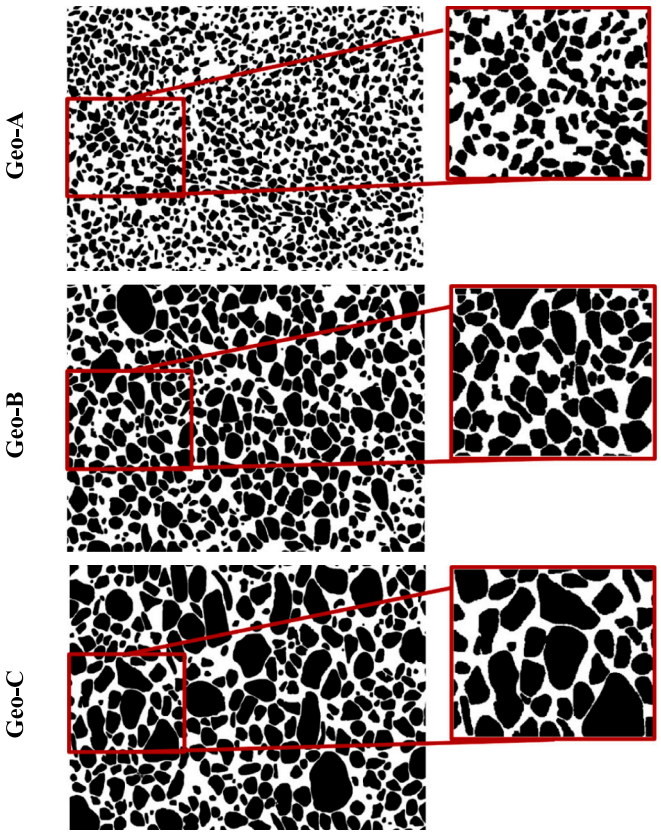

Fig. 2. Pore geometries used in the microfluidic experiments.

inspected and satisfied without the need for data transformation. The results indicate a significant variation in the pore aspect ratio distributions with a p-value of 0.00086, confirming that the distributions differ meaningfully across the geometries.

Fig. 4 illustrates the distribution of throat sizes along the initial sections of the flow direction for three micromodel geometries (Geo-A, Geo-B, and Geo-C). Each section width corresponds to the median grain size of the respective geometry. The box plots display the range of throat sizes within these sections, allowing for a comparison of the initial throat dimensions that MPs encounter upon entering each system. These throat dimensions will be referred to as the "initial throats" in the system throughout the following discussion.

The quantification of MPs accumulation was based on image analysis of a specific area of interest within the micromodel geometry. The entire micromodel geometry was derived from a 3D image of a sand pack, designed to represent a representative elementary volume (REV) of porosity for the system. Within this geometry, a subset was chosen as the area of interest to ensure an open boundary condition and reduce the influence of boundary effects on the observed behavior. Boundary effects in micromodel experiments can significantly impact particle retention and transport, particularly near the edges of the domain where fluid dynamics are altered by the physical limits of the system. By selecting an area away from the boundaries, the study ensured that the observed MPs behaviors were driven by the internal dynamics of the porous media rather than by artificial constraints at the domain edges. This selection also allowed MPs to flow from multiple directions during the desaturation process, better mimicking natural systems where particles experience complex and dynamic flow pathways. Additionally, the area of interest was chosen to achieve a camera resolution of 1 μm, enabling accurate tracking and segmentation of individual MPs. The selected areas were fixed and consistent across all experimental runs and geometries to ensure the validity and comparability of the observed results.

2.3. Experimental procedure

Fig. 5 shows the micromodel experimental setup used to study the behavior of MPs. Micromodel inlets were connected to two precision syringe pumps (Kats Scientific, NE-1010) via 0.25 mm internal diameter PEEK flow lines, allowing both the injection and withdrawal of MPs suspensions, corresponding to saturation and desaturation respectively.

Table 1
Properties of the micromodels used in the study.

Geo-	Φ -	D_{10} (μm)	D_{60} (μm)	D_{50} (μm)	D_P (μm)	D_T (μm)	D_P/D_T -	θ_G (°)	U_c -	SA_G (mm^2)	Z -
A	0.451	60.46	117.59	109.81 ± 37.78	74.30 ± 49.14	59.84 ± 33.39	1.17 ± 1.06	21.20 ± 2.80	1.94	3.06	2.78
B	0.292	73.92	179.59	161.83 ± 64.74	80.50 ± 42.98	43.52 ± 77.23	1.85 ± 3.44	41.84 ± 55.18	2.43	2.77	2.56
C	0.269	63.50	180.54	156.01 ± 103.0	95.29 ± 48.70	65.28 ± 113.47	1.46 ± 2.64	84.75 ± 42.01	2.84	1.89	2.23
Φ: Porosity				D_{10}: 10-Percentile Grain Size				D_{60}: 60-Percentile Grain Size			
D_{50}: Grain Median Size				D_P: Pore Median Size				D_T: Throats Median Size			
D_P/D_T: Pore Aspect Ratio				θ_G: Grain Orientation Angle				U_c: uniformity coefficient			
SA_G: Grain Surface Area				Z: Pore Coordination Number							

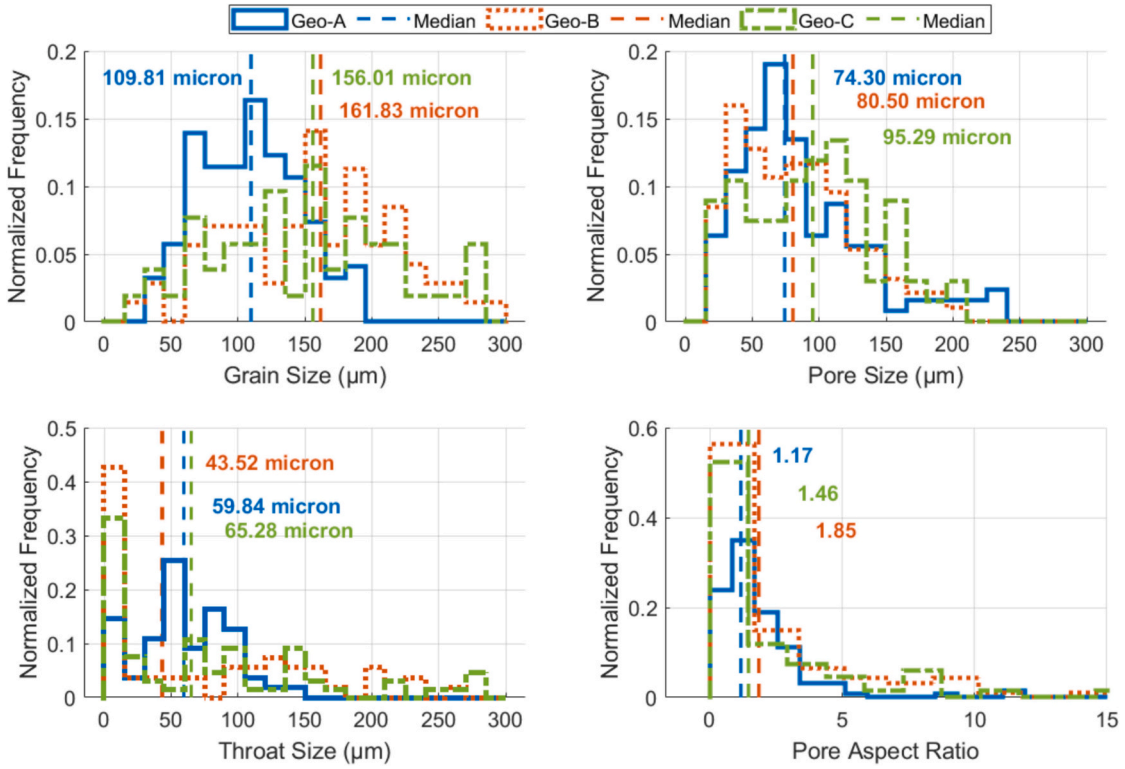

Fig. 3. Probability distributions of grain size, pore size, throat size, and pore aspect ratio for the three analyzed geometries (Geo-A, Geo-B, and Geo-C). The vertical dashed lines indicate the median values for each distribution.

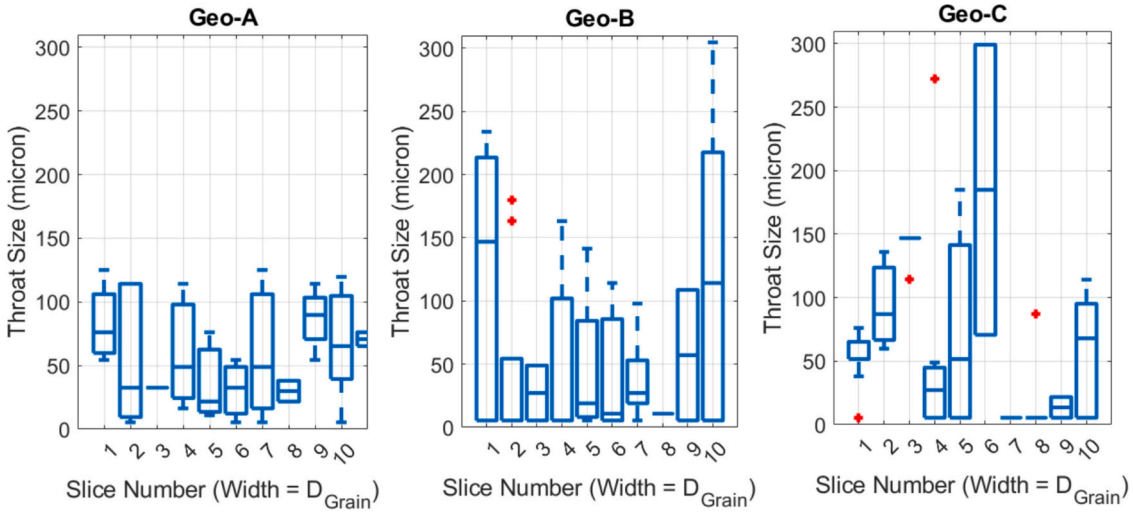

Fig. 4. Throat size distribution in the initial sections of the flow paths for the micromodel geometries used in the study, with section widths corresponding to the median grain size.

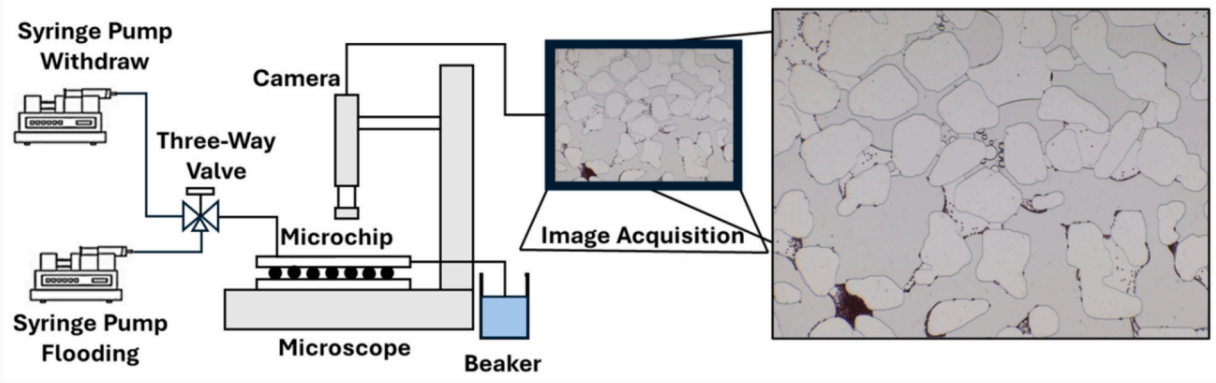

Fig. 5. Illustration of the micromodel experimental setup for MPs retention in porous media study.

Another PEEK flow line was connected to the micromodel outlet at atmospheric pressure and placed in a beaker to collect the produced effluent. Prior experimental flooding, the micromodels underwent flushing by injecting 5 mL ethanol followed by 30 mL of deionized water to remove contaminants. Subsequently, air was introduced into the micromodels until all residual ethanol / DI water was removed.

Three distinct MPs suspensions and three pore geometries were subjected to flooding experiments, resulting in a total of nine experimental runs. Each run consisted of one complete cycle of saturation and desaturation, with each phase involving the injection or withdrawal of fluid equivalent to 8 pore volumes. The term "pore volumes" refers to the amount of fluid required to completely fill the pore space of the porous geometry. This value was selected based on preliminary experiments, which identified 8 pore volumes as sufficient to achieve complete saturation of the porous geometry during the saturation phase. Once saturation was achieved, the injection was stopped, and the desaturation phase began, during which fluid was withdrawn using suction pressure applied by the withdrawal pump. The consistent use of 8 pore volumes across all experimental runs ensured uniformity and facilitated comparability of the results.

During the saturation phase, the MPs suspension was introduced into the micromodel at a controlled flow rate of 3 μL/min, corresponding to a velocity of 0.05 cm/s. This flow rate was selected to align with reported subsurface flow velocities in porous coastal sediments and intertidal zones, ranging from 0.02 to 0.35 cm/s, under tidal dynamics (Heiss et al., 2017; Røy et al., 2008; Santos et al., 2012) By maintaining this flow rate, the experiments ensured stable and consistent injection of MPs, allowing for the observation of retention and transport behaviors under conditions relevant to subsurface and coastal porous media. The desaturation phase followed the saturation phase and involved the controlled withdrawal of the suspension using suction pressure applied by the withdrawal pump. No additional MPs were introduced during this phase, instead, the suction process induced the fluid to move from the entire micromodel, causing the MPs already in the system to travel through the porous media to the area of interest. The same flow rate was used during desaturation to ensure consistency across experiments and comparability of results. Continuous imaging was performed throughout both phases at a rate of 12 frames per minute, with a 2.5× zoom, achieving a spatial resolution of 1 μm per pixel to enable clear identification of individual microspheres.

Each experimental condition was performed once in this study to evaluate the transport and retention behaviors of MPs under specific scenarios. While duplication of experiments was not conducted, the behavior of the mixed suspension, containing both hydrophobic and hydrophilic MPs, serves as a statistical validation for the trends observed in individual suspensions. However, future studies should incorporate duplicated runs to further enhance the reproducibility of the results.

2.4. Image processing

Micromodel experiments were imaged using a Leica Z6 APO monocular macroscope, equipped with a high-precision stage offering an XY positional accuracy of 1 μm. Imaging was conducted with a Leica MC170 HD RGB camera, which captures images at a resolution of 2592 × 1944 pixels. Images were continuously captured throughout saturation and desaturation cycles of each experimental run.

Dry pore system images were acquired before each experiment to create masks that distinguished grains from pore spaces, effectively isolating collector surfaces for MPs attachment. During each experimental run, nine images were selected from each stage (i.e., saturation and desaturation) totaling 18 images per experimental run. These images were segmented and analyzed to ensure quantitative validation of visual observations.

With the pore space separated from the grains, the subsequent segmentation process focused on identifying the air, water, and MPs phases based on their unique properties. The air phase was identified by detecting high-gradient values at the AWI, while minimizing interference from the generally low gradient between air and water. MPs were segmented by identifying pixel clusters within a defined color range (i.e., ±15 from the dominant MPs color), with unclassified areas designated as the water phase. The segmentation was performed using Pergeos software, which generated classified images with four distinct phases: air, water, grains, and MPs.

To further analyze these classifications, four copies of each segmented image were created: Air and Grain classes, Grains and Water classes, Air and Water classes, and the fourth contained the MPs class only. Binary images representing the ASI, WSI, and AWI were generated from the first three copies using the Label Interfaces function in Pergeos. These binary images were combined with the MPs-only image using the AND function to identify MPs attached to specific interfaces. To enhance detection accuracy, interface regions were dilated by 5 pixels prior to analysis.

The Volume Fraction function was used to quantify the pixel counts of each phase, providing detailed metrics of MPs distribution and attachment across different interfaces. This systematic approach ensured a comprehensive evaluation of MPs retention behaviors under varying experimental conditions. Fig. 6 presents segmentation results for the three micromodel geometries, illustrating the differentiation of interfaces and MPs attachment.

3. Results and discussion

3.1. Impact of hydrophobicity: visual observations

Fig. 7 illustrates the retention mechanisms of MPs within the pore structure of Geo-A, highlighting the impact of hydrophobicity on the MPs attachment and distribution within the pore system. Three stages in

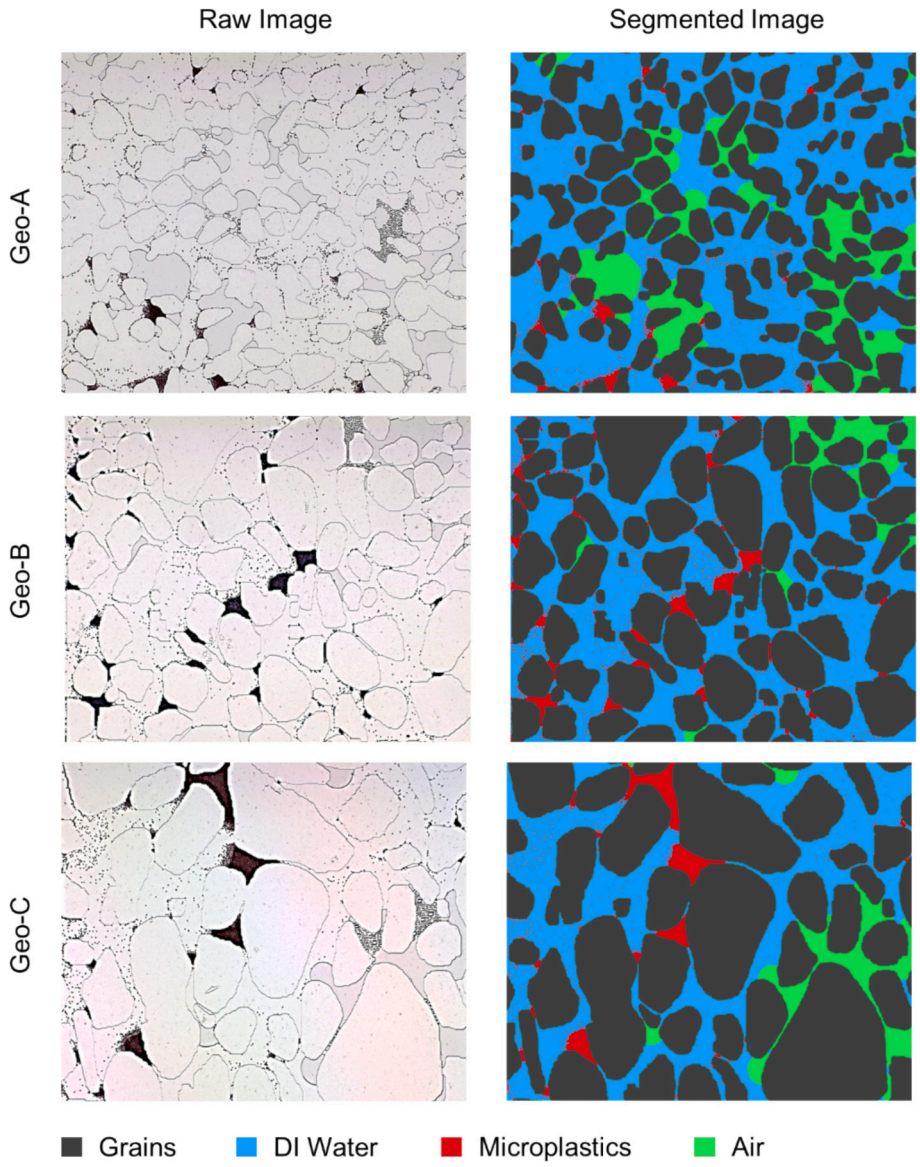

Fig. 6. Illustration of image segmentation obtained from microfluidic images of Geo-A, Geo-B and Geo-C.

the experimental sequence are shown for each hydrophobicity case: (1) breakthrough retention, upon injecting between 4 and 6 pore volumes, marking the initial phase of MPs retention; (2) end of saturation retention, upon injecting 8 pore volumes, representing the conditions before desaturation phase begins; and (3) end of desaturation retention, upon injecting 16 pore volumes. Each stage provides insight into the distinct behaviors of MPs across hydrophilic, hydrophobic, and mixed conditions.

For hydrophilic MPs, breakthrough retention reveals a tendency for particles to aggregate and travel as clusters, as seen in Fig. 7a. This clustering behavior is driven by the low energy barrier, as indicated in the DLVO energy profile (Fig. 1a), which facilitates attachment both among MPs and to grain surfaces, as shown in Fig. 1b. Two primary retention mechanisms emerge at this stage: large MPs clusters become sieved within smaller throats along the primary flow paths, while additional MPs attach to the SWI. This observation of hydrophilic MPs forming clusters due to low energy barriers is consistent with findings by Zhao et al. (2022), which showed that aggregation of colloidal microplastic particles (CMPs) were promoted aggregation under favorable energy conditions. As pore volume injection progresses towards the end of the saturation phase, MPs that have accumulated within the smaller throats redirect the flow to neighboring paths causing further throats clogging, leading to MPs accumulation in pores with lower throat connectivity (Fig. 7b), these observations align with the findings in (Elrahmani and Al-Raoush, 2024). By the end of the desaturation phase, as depicted in Fig. 7c, larger throats remain open, enabling air phase penetration through these flow paths. This airflow sweeps some MPs from the SWI and transports them to previously clogged throats, where they accumulate with retained MPs, ultimately obstructing additional air flow through these channels.

For hydrophobic MPs, the breakthrough retention phase (Fig. 7d) demonstrates a different attachment mechanism, where MPs predominantly adhere to grain surfaces along the SWI, especially on surfaces facing the flow direction. The observed preferential attachment of hydrophobic MPs to grain surfaces along the SWI aligns with results presented in the literature, which demonstrated that hydrophobicity enhances attachment efficiency, particularly in systems with high specific surface areas (Anastopoulos et al., 2022; Wang et al., 2022b). As saturation increases, MPs near the throats begin to bridge by attaching to one another, which initiates the clogging of smaller throats through the formation of interconnected MPs structures. Fig. 7e illustrates the bridging of MPs at the smaller throats beside continuing to attach to

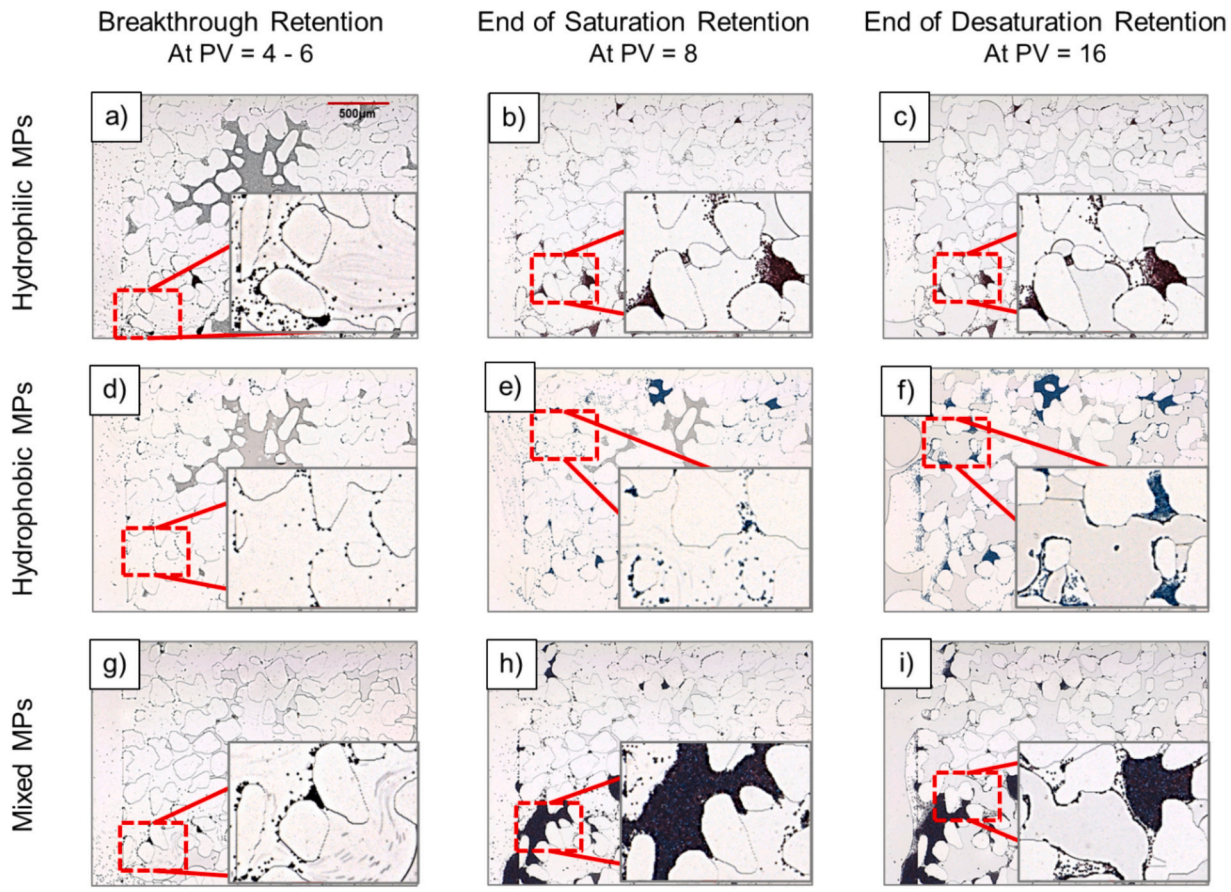

Fig. 7. Pore-scale images from the microfluidic chip of Geo-A to illustrate the retention mechanisms of different microplastic hydrophobicity.

available sites on grain surfaces. By the end of desaturation (Fig. 7f), MPs that primarily attached to grain surfaces, rather than clogging the throats as in the case of hydrophilic MPs, leave multiple throats open, permitting air phase entry. This airflow enhances the available attachment sites for MPs at the AWI. The surface chemistry of hydrophobic MPs further increases their tendency to adhere to the AWI, promoting additional retention during desaturation.

The mixed hydrophobicity MPs exhibit a blend of behaviors seen with both hydrophilic and hydrophobic MPs. During breakthrough retention (Fig. 7g), MPs cluster and simultaneously attach to available SWI sites, reflecting both the sieving effect in smaller throats and a preference for SWI attachment. As saturation increases, a combination of clustering, throat clogging and attachment to SWI creates high-density MPs accumulations in pore spaces (Fig. 7h). Mixed MPs take advantage of the retention mechanisms of both hydrophilic and hydrophobic particles, resulting in MPs accumulation in pores surrounded by smaller throats and larger grain surfaces that favor attachment. By the end of desaturation (Fig. 7i), MPs accumulated in the pore spaces low-connectivity pores remain inaccessible to the air phase, while the air bypasses these zones and reaches higher-connectivity pores, leading to additional MPs attachment at the AWI within these more accessible areas.

3.2. Impact of geometry: visual observations

Fig. 8 illustrates the retention mechanisms of mixed hydrophobicity MPs within the pore structures of Geo-A, Geo-B, and Geo-C, highlighting the impact of pore geometries on MPs attachment and distribution at three distinct stages in the experimental sequence: (1) breakthrough retention, (2) end of saturation retention, and (3) end of desaturation retention. To better understand the effects of geometry on MPs retention, the observations focus on comparing these geometries at each stage rather than tracing each geometry individually from start to finish.

During breakthrough retention, two primary mechanisms drive MPs retention: the clustering and sieving of MPs within smaller throats, and attachment to the SWI. Retention at this stage is influenced by both the initial presence of smaller throats and the availability of attachment sites on the SWI. As shown in Fig. 4, Geo-A and Geo-C are characterized by smaller initial throat sizes, resulting in higher MPs retention in the pore throats compared to Geo-B (observed in Fig. 8a and g relative to Fig. 8d). Attachment to the SWI also varies according to the grains specific surface area, as geometries with higher specific surface areas provide more attachment sites. This can be observed in Geo-A and Geo-B, which exhibit higher SWI attachment due to their larger grain specific surface areas (Table 1), thereby enhancing MPs retention through increased attachment sites in the initial stages.

At the end of the saturation phase, the influence of smaller throats becomes more apparent as they continue to govern flow paths and MPs retention. In geometries with initially smaller throats, such as Geo-A and Geo-C, early clogging forces the flow to divert to adjacent paths. This diversion leads to additional clogging around the same pore, resulting in significant MPs accumulation in pores with restricted connectivity, as shown in Fig. 8b and h. The enhanced retention of MPs in smaller throats, as observed in this study, is consistent with findings by Li et al. (2024), which demonstrated that porous media with restricted flow paths amplify microplastic deposition due to localized clogging. Smaller throat size as well as smaller pore to throat size ratio are responsible for this observation. In contrast, Geo-B (Fig. 8e) demonstrates a different retention pattern. With larger initial throat sizes and a higher standard deviation in throat distribution (Fig. 4), Geo-B requires more pore volume to achieve clogging in the early flow paths through sieving, allowing MPs to divert into larger throats without initiating clogging.

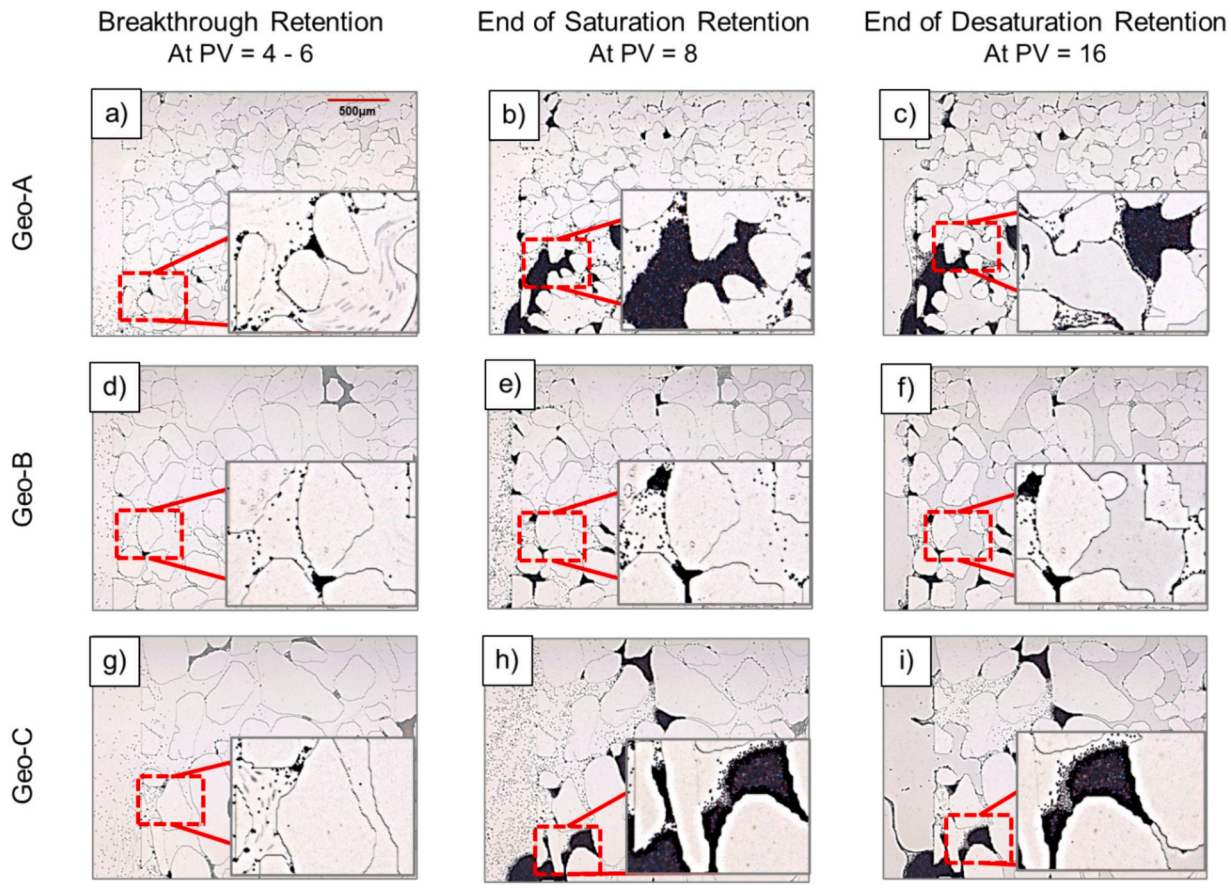

Fig. 8. Pore-scale images from the microfluidic chips of Geo-A, Geo-B and Geo-C as an illustration of the retention mechanisms of microplastic in different pore geometries.

Moreover, in Geo-A, the abundance of attachment sites along the SWI leads to more severe MPs accumulation, as both sieving and bridging contribute to the retention dynamics in this geometry, as observed in Fig. 8b.

In the end of desaturation stage, pore connectivity emerges as the dominant factor influencing retention. Low-connectivity geometries, such as Geo-C, restrict air phase penetration, thereby limiting AWI attachment opportunities. As seen in Fig. 8i, the low connectivity in Geo-C prevents the air phase from reaching accumulated MPs in the pores, resulting in minimal attachment at the AWI. By contrast, in Geo-A (Fig. 8c), higher pore connectivity allows the air phase to penetrate through the system more effectively, facilitating extensive MPs attachment at the AWI compared to Geo-C. Geo-B, on the other hand, presents a different behavior where the majority of throats remain unclogged by the end of saturation, limiting MPs accumulation and enabling the air phase to flow freely through the system as shown in Fig. 8f. Consequently, Geo-B demonstrates increased MPs attachment at both the AWI and ASI.

3.3. Attachment profiles of microplastics

This section presents a transition from the qualitative visual observations of MPs retention to the quantitative analysis of MPs attachment profiles across different pore geometries and hydrophobicity cases. Fig. 9 illustrates the fraction of MPs attached to various interfaces within the pore system (i.e., AWI, ASI, SWI, and other MPs) during three critical stages of retention: breakthrough, end of saturation, and end of desaturation. The goal is to validate the visual observations through quantitative measures of attachment and to compare the behavior of MPs retention in different pore geometries in terms of MPs distribution across these interfaces. Values shown in Fig. 9 represent the percentage of MPs retained on each interface relative to the total number of retained MPs at each stage.

For hydrophilic MPs, the breakthrough retention stage (Fig. 9a) shows a predominant attachment of MPs to each other (MPs-MPs attachment), with minimal attachment to the SWI and negligible attachment to the AWI. This aligns with visual observations (Fig. 7a), where hydrophilic MPs tended to cluster and were retained by sieving in the smaller throats of the system. This clustering is particularly pronounced in geometries with smaller initial throats, such as Geo-C as illustrated in Fig. 4, where the MPs-MPs attachment is 88 %, which experience more intense MPs sieving due to narrower flow path. By the end of the saturation phase (Fig. 9b), the attachment profile shifts, with a higher percentage of MPs adhering to the SWI. This shift is attributed to clogging of the primary throats, which redirects flow and causes MPs to accumulate in pores where they have increased contact with grain surfaces, as observed in Fig. 7b. At the end of the desaturation phase (Fig. 9c), the attachment profile for geometries with lower pore connectivity, Geo-C, remains relatively stable. In contrast, in higher-connectivity pore space, Geo-A, where 39 % of the retained MPs are attached to the AWI, supporting the observations in Fig. 7c, where the air phase sweeps MPs from the SWI and transports them to previously clogged throats.

For hydrophobic MPs, the breakthrough retention phase (Fig. 9d) reveals a distinct attachment pattern compared to hydrophilic MPs, with MPs showing a higher affinity for the SWI and AWI than for MPs-MPs attachment. This attachment preference is consistent with the hydrophobic nature of the MPs, which promotes adhesion to grain surfaces rather than clustering, as observed in Fig. 7d. Geometries with higher grain specific surface area display more attachment to the SWI, as

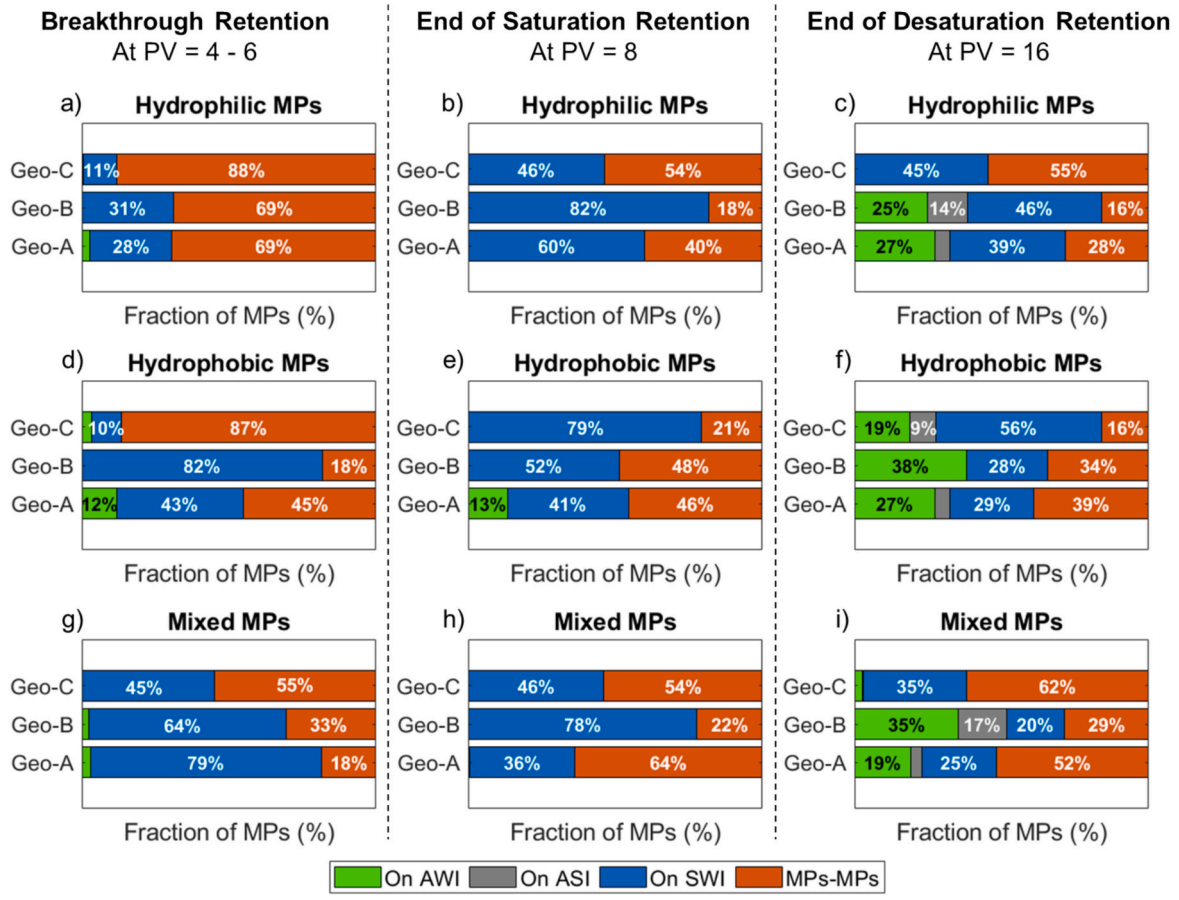

Fig. 9. Attachment profiles of the retained microplastics during saturation-desaturation cycle.

observed for Geo-B where 82 % of the retained MPs are attached to the SWI. By the end of saturation (Fig. 9e), the attachment profile indicates an increase in MPs-MPs attachment due to bridging, which gradually blocks smaller throats, as seen in Fig. 7e. Notably, the percentage of MPs attached to the AWI remains relatively stable at this stage, indicating that bridging occurs primarily within the water phase. In the desaturation phase (Fig. 9f), the attachment profile shifts further towards the AWI, reflecting the increased availability of air-exposed attachment sites as the air phase penetrates through open flow paths. This behavior contrasts with the hydrophilic case (Fig. 9c), where AWI attachment was limited. The increased attachment of hydrophobic MPs to the air-water interface (AWI) is primarily driven by their surface chemistry, which promotes retention at the AWI. This behavior is further facilitated by the free flow of air through unclogged throats, resulting in a higher proportion of AWI attachment in all three geometries compared to hydrophilic MPs (e.g., 38 % vs. 25 % in Geo-B), as illustrated in Fig. 7f.

For mixed MPs, the breakthrough retention stage (Fig. 9g) shows a combined retention behavior influenced by both hydrophilic and hydrophobic properties. MPs attach significantly to the SWI, with the degree of attachment correlating to the grain specific surface area, which provides more attachment sites in geometries such as Geo-A and Geo-B, 79 % and 64 % respectively. This observation supports the behaviors shown in Fig. 8a, d, and g, where both clustering and SWI attachment were observed, with Geo-A and Geo-B exhibiting more SWI attachment. By the end of the saturation phase (Fig. 9h), the attachment profile in geometries with smaller initial throats, such as Geo-A, shifts towards MPs-MPs attachment. This shift is due to clogging from sieving and bridging within smaller throats, where MPs accumulate in close proximity, as observed in Fig. 8b and h. For geometries with larger initial throats (e.g., Geo-B, as demonstrated in Fig. 4) SWI attachment remains the dominant mechanism, as larger throats reduce the likelihood of clogging and allow MPs to reach and attach to grain surfaces more freely.

At the end of the desaturation phase (Fig. 9i), the attachment profile for mixed MPs shows no significant attachment to the AWI in low-connectivity pore spaces (i.e., Geo-C) has only 3 % attachment to the AWI. However, in higher-connectivity pore space, (i.e., Geo-A) some attachment to the AWI is observed, although at a lower percentage than in the hydrophobic case. This selective AWI attachment is particularly evident in Geo-B (Fig. 8f) with 35 % attachment to AWI and 17 % to the ASI, where larger initial throats (Fig. 4) facilitate air phase penetration without causing extensive throat clogging, allowing MPs to attach to the AWI in open flow paths.

Considering the discussion above, Table 2 below summarizes the

Table 2
Summary of observed MPs retention mechanisms.

MPs	Breakthrough retention	End of saturation retention	End of desaturation retention
Hydrophilic	Clustering and Sieving at Smaller Throats (Figs. 7a, 9a)	Accumulation at Lower Connectivity Pores (Figs. 7b, 9b)	Attachment to AWI and Sweeping Toward Clogged Throats (Figs. 7c, 9c)
Hydrophobic	Attachment to Available Sites of SWI and AWI (Figs. 7d and 9d)	Bridging and Accumulation at Throats (Figs. 7e and 9e)	Attachment to AWI at the Open Pores (Figs. 7f and 9f)
Mixed	Clustering and Sieving and Attachment to SWI (Figs. 7g, 9g)	Accumulation at Pore Space (Figs. 7h and 9h)	Attachment to AWI at Higher Connectivity Pores (Figs. 7i and 9i)

observed MPs retention mechanisms for each hydrophobicity case (i.e., hydrophilic, hydrophobic, and mixed MPs) across the three key stages: breakthrough retention, end of saturation retention, and end of desaturation retention.

3.4. Overall retention behavior

The quantitative results for the retention percentage of MPs during pore volume injection are presented in this section during the saturation-desaturation cycle. The retention percentage is defined as the ratio of MPs retained within the system at a given pore volume to the total MPs injected at that pore volume. The plots in Fig. 10 illustrate the retention curves for the nine experimental cases as functions of pore volume, with each curve depicting the progression through saturation followed by desaturation. The initiation of MPs retention mechanisms typically occurs after the injection of approximately four pore volumes, the point referred to as the breakthrough retention. This marks the onset of MPs being captured within the pore structure.

For hydrophilic MPs, retention at breakthrough is inversely related to the pore aspect ratio. Geometries with smaller pore aspect ratios, such as Geo-A (illustrated in Fig. 3), exhibit higher initial retention values. The observation that smaller pore to throat ratios enhance clustering and sieving during breakthrough retention is supported by He et al. (2023), who showed that retention mechanisms in microfluidic experiments are strongly influenced by pore-throat geometry, with smaller ratios increasing particle retention. By the end of the saturation phase, geometries with smaller initial throat sizes and lower pore connectivity, such as Geo-C, retain a greater proportion of MPs, around 25 %, largely due to accumulation in low-connectivity pores. Conversely, Geo-B, characterized by a higher pore aspect ratio and larger initial throat sizes, demonstrates minimal retention. At the end of desaturation, despite a shift in the attachment profile towards increased AWI attachment in open pores, as observed in Fig. 9c, the overall retention percentage within the porous media remains stable. Mainly because the MPs retained originally in the system are clogging the main flow paths.

For hydrophobic MPs, breakthrough retention shows a positive correlation with grain specific surface area. Geometries with higher grain surface areas, such as Geo-A and Geo-B, retain more MPs initially, likely due to the MPs' affinity for attaching to the SWI. By the end of saturation, geometries with grains oriented closer to the flow direction and smaller initial throat sizes, such as Geo-A, retain around 40 % of the MPs injected. This orientation enhances bridging of MPs as more grain surface is exposed around the throats, which facilitates attachment of MPs to the SWI in the throats and subsequent clogging of throats. In contrast, Geo-C, with a lower grain surface area and grains oriented perpendicularly to the flow, exhibits minimal retention, <5 %. At the end of desaturation, attachment profiles show a slight increase in AWI interaction, as observed in Fig. 9f, yet the overall retention remains nearly unchanged. Geo-A demonstrates a minor release of MPs, as some particles attach to the AWI at the open pores and move through the system.

For mixed MPs, breakthrough retention begins at earlier in geometries with larger grain surface areas, like Geo-A, indicating that SWI attachment drives early retention more strongly than clustering and sieving. By the end of saturation, Geo-A retains more MPs, around 50 %, compared to both the hydrophobic, 40 %, and hydrophilic, 20 %, cases due to the combination of high grain surface area and smaller initial throat sizes, which enhances both SWI attachment and MPs clustering.

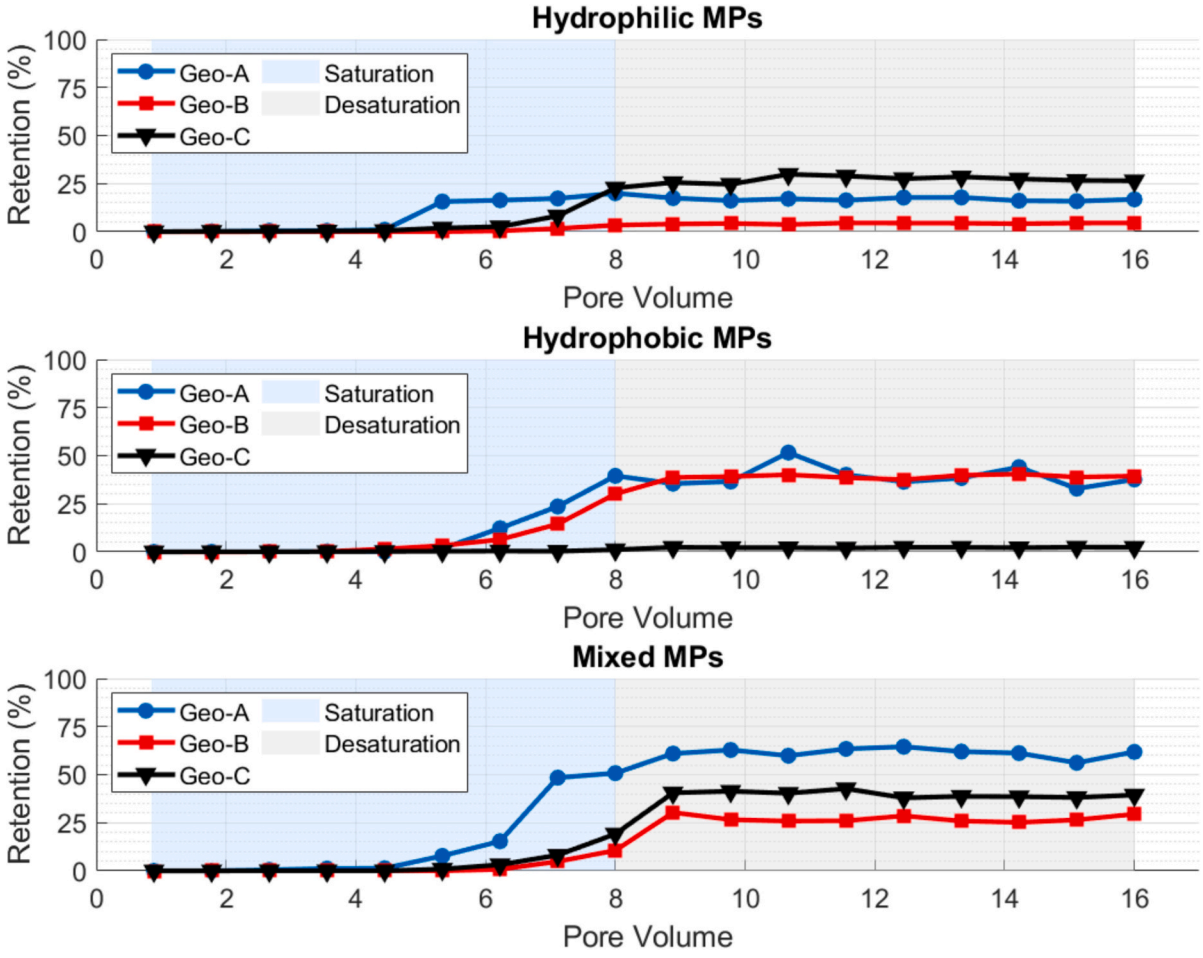

Fig. 10. Fraction of microplastics retained in the system as a function of pore volume during saturation-desaturation cycle.

At the end of desaturation, retention percentages across geometries remain consistent, with no significant change in MPs retention. This stability underscores the strong retention forces within the system that prevent MPs release even in the presence of air.

Notably, for all the cases the presence of air during the desaturation phase does not facilitate significant release of MPs, regardless of their hydrophobicity, highlighting the strong retention forces within the system.

These findings have significant environmental implications, particularly in the context of subsurface contamination and groundwater quality. The retention behaviors observed for different MPs highlight the complexity of their transport and potential risks in natural and engineered systems.

Hydrophilic MPs, with their strong clustering and minimal mobility during desaturation, are likely to persist in fine-grained sediments, creating contamination hotspots. These zones pose a risk for prolonged leaching of associated pollutants, such as heavy metals and organic compounds, contributing to long-term degradation of water quality. Conversely, hydrophobic MPs exhibit higher mobility in high-connectivity porous media, increasing their likelihood of migrating into larger water systems. Their strong interaction with the air-water interface (AWI) suggests that even minor fluctuations in the water table or air intrusion can redistribute MPs, posing additional risks to connected water bodies.

The dual retention behavior of mixed MPs further complicates the prediction of their transport and retention in natural systems. Their ability to exploit multiple retention mechanisms makes them particularly persistent under diverse environmental conditions, requiring advanced modeling to better understand their migration pathways and contamination potential. The persistence of MPs during desaturation cycles indicates that natural flushing processes, such as seasonal water table fluctuations, may have limited efficiency in mitigating MPs contamination.

These insights are particularly relevant for wastewater treatment systems. Retained MPs can serve as vectors for contaminants, including hydrophobic organic compounds and heavy metals, thereby amplifying their environmental impact and prolonging their residence time in the subsurface. This underscores the need for targeted mitigation strategies, such as the design of engineered filtration systems or infiltration basins optimized for specific MP properties and pore geometries. Such approaches would enhance the efficiency of retention and removal, mitigating the long-term risks posed by MPs in subsurface and wastewater environments.

4. Conclusions

This study investigated the effects of microplastics (MPs) hydrophobicity and pore geometry on MPs retention mechanisms in porous media during saturation-desaturation cycles. Using controlled microfluidic experiments, the study systematically analyzed how variations in MPs surface chemistry and pore structure influence retention behavior under dynamic pore volume injections. Quantitative measurements were used to examine MPs distribution across the SWI, AWI, and ASI interfaces.

Hydrophilic MPs were primarily retained through clustering and sieving mechanisms, driven by low energy barriers to attachment. Retention reached up to 25 % by the end of saturation, predominantly in smaller throats within low-connectivity geometries. Clustering and sieving caused pore-scale clogging, diverting flow to adjacent pathways and increasing MPs accumulation in stagnant zones. During desaturation, hydrophilic MPs exhibited minimal movement (<10 % displacement), reflecting strong retention forces and limited AWI interaction.

Hydrophobic MPs displayed distinct behaviors, with over 50 % attachment to the SWI by the end of saturation and 38 % attachment to the AWI by the end of desaturation. In high-connectivity geometries, hydrophobic MPs formed bridging networks across throats, increasing retention to 40 %. Subdividing air bubbles during desaturation enhanced AWI area, facilitating redistribution and further attachment.

Mixed MPs combined retention mechanisms of hydrophilic and hydrophobic MPs. Early in saturation, 79 % attached to the SWI, particularly in high-surface-area media, with retention reaching 50 %. Over time, clustering and sieving shifted attachment profiles, increasing MPs-MPs attachment to 64 %, leading to dense accumulations. Mixed MPs persisted with negligible desaturation-driven release, posing challenges for natural remediation.

These findings highlight significant environmental risks, especially for subsurface contamination and groundwater quality. Hydrophilic MPs persist in fine-grained sediments, forming hotspots for prolonged pollutant leaching, while hydrophobic MPs are more mobile in high-connectivity media, increasing risks of migration into larger systems. Their strong interaction with the AWI allows redistribution during minor water table fluctuations, exacerbating contamination. Mixed MPs, with dual retention mechanisms, are highly persistent, complicating transport predictions. The ineffectiveness of natural flushing processes underscores the need for targeted mitigation strategies, such as filtration systems tailored to MP properties and pore geometries. Future research should investigate the long-term retention of MPs under repeated saturation cycles and their interactions with co-contaminants to inform remediation strategies and reduce environmental impact.

CRediT authorship contribution statement

Ahmed Elrahmani: Writing – original draft, Validation, Formal analysis, Data curation. **Riyadh I. Al-Raoush:** Writing – original draft, Supervision, Resources, Project administration, Methodology, Investigation, Funding acquisition, Conceptualization. **Jamal A. Hannun:** Writing – review & editing, Visualization, Methodology, Formal analysis. **Mhd. Taisir Albaba:** Writing – review & editing, Methodology, Investigation. **Thomas D. Seers:** Writing – review & editing, Methodology, Funding acquisition.

Declaration of competing interest

The authors declare that they have no known competing financial interests or personal relationships that could have appeared to influence the work reported in this paper.

Acknowledgment

This publication was made possible by an Academic Research Grant supported by Qatar Research Development and Innovation Council ARG01-0430-230041. Jamal Hannun was supported by GSRA7 1-0217-20002 from the Qatar National Research Fund (QNRF), which is a part of Qatar Research Development and Innovation Council (QRDI). The content is solely the responsibility of the authors and does not necessarily represent the official views of Qatar Research Development and Innovation Council. The authors would like to thank the Center for Advanced Materials (CAM) at Qatar University for help in Zeta Potential Analysis. Open Access funding provided by the Qatar National Library.

Appendix A. Supplementary data

Supplementary data to this article can be found online at https://doi.org/10.1016/j.scitotenv.2025.179238.

Data availability

Data will be made available on request.

References

Al-Raoush, R., 2012. Change in microstructure parameters of porous media over representative elementary volume for porosity. Part. Sci. Technol. 30. https://doi.org/10.1080/02726351.2010.543262.

Anastopoulos, I., Pashalidis, I., Kayan, B., Kalderis, D., 2022. Microplastics as carriers of hydrophilic pollutants in an aqueous environment. J. Mol. Liq. 350. https://doi.org/10.1016/j.molliq.2021.118182.

Bergendahl, J., Grasso, D., 2000. Prediction of colloid detachment in a model porous media: hydrodynamics. Chem. Eng. Sci. 55. https://doi.org/10.1016/S0009-2509(99)00422-4.

Bradford, S.A., Kim, H., 2012. Causes and implications of colloid and microorganism retention hysteresis. J. Contam. Hydrol. 138–139. https://doi.org/10.1016/j.jconhyd.2012.06.007.

Bradford, S.A., Leij, F.J., 2018. Modeling the transport and retention of polydispersed colloidal suspensions in porous media. Chem. Eng. Sci. 192. https://doi.org/10.1016/j.ces.2018.08.037.

Bradford, S.A., Torkzaban, S., 2015. Determining parameters and mechanisms of colloid retention and release in porous media. Langmuir 31. https://doi.org/10.1021/acs.langmuir.5b03080.

Bradford, S.A., Torkzaban, S., Wiegmann, A., 2011. Pore-scale simulations to determine the applied hydrodynamic torque and colloid immobilization. Vadose Zone J. 10. https://doi.org/10.2136/vzj2010.0064.

Chen, C., Packman, A.I., Zhang, D., Gaillard, J.F., 2010. A multi-scale investigation of interfacial transport, pore fluid flow, and fine particle deposition in a sediment bed. Water Resour. Res. 46. https://doi.org/10.1029/2009WR009018.

De Souza MacHado, A.A., Lau, C.W., Till, J., Kloas, W., Lehmann, A., Becker, R., Rillig, M.C., 2018. Impacts of microplastics on the soil biophysical environment. Environ. Sci. Technol. 52. https://doi.org/10.1021/acs.est.8b02212.

Dichgans, F., Boos, J.P., Ahmadi, P., Frei, S., Fleckenstein, J.H., 2023. Integrated numerical modeling to quantify transport and fate of microplastics in the hyporheic zone. Water Res. 243. https://doi.org/10.1016/j.watres.2023.120349.

Dong, Z., Qiu, Y., Zhang, W., Yang, Z., Wei, L., 2018. Size-dependent transport and retention of micron-sized plastic spheres in natural sand saturated with seawater. Water Res. 143. https://doi.org/10.1016/j.watres.2018.07.007.

Dong, S., Zhou, M., Su, X., Xia, J., Wang, L., Wu, H., Suakollie, E.B., Wang, D., 2022a. Transport and retention patterns of fragmental microplastics in saturated and unsaturated porous media: a real-time pore-scale visualization. Water Res. 214. https://doi.org/10.1016/j.watres.2022.118195.

Dong, S., Zhou, M., Su, X., Xia, J., Wang, L., Wu, H., Suakollie, E.B., Wang, D., 2022b. Transport and retention patterns of fragmental microplastics in saturated and unsaturated porous media: a real-time pore-scale visualization. Water Res. 214. https://doi.org/10.1016/j.watres.2022.118195.

Elrahmani, A., Al-Raoush, R.I., 2024. Spatial dependency of clogged throats in porous media: a microscale investigation. SPE J. 1–17. https://doi.org/10.2118/223975-PA.

Elrahmani, A., Al-Raoush, R.I., Abugazia, H., Seers, T., 2022. Pore-scale simulation of fine particles migration in porous media using coupled CFD-DEM. Powder Technol. 398, 117130. https://doi.org/10.1016/j.powtec.2022.117130.

Elrahmani, A., Al-Raoush, R.I., Seers, T.D., 2023. Clogging and permeability reduction dynamics in porous media: a numerical simulation study. Powder Technol. 427, 118736. https://doi.org/10.1016/j.powtec.2023.118736.

Elrahmani, A., Al-Raoush, R.I., Ayari, M.A., 2024. Modeling of permeability impairment dynamics in porous media: a machine learning approach. Powder Technol. 433. https://doi.org/10.1016/j.powtec.2023.119272.

Esfandiari, A., Abbasi, S., Peely, A.B., Mowla, D., Ghanbarian, M.A., Oleszczuk, P., Turner, A., 2022. Distribution and transport of microplastics in groundwater (Shiraz aquifer, southwest Iran). Water Res. 220. https://doi.org/10.1016/j.watres.2022.118622.

Fang, Y., Kong, L., Zhang, P., Zhang, L., Zhao, H., Xiang, X., Cheng, S., Zhang, H., Ju, F., Li, L., 2022. Fifteen-year analysis of constructed wetland clogging: a critical review. J. Clean. Prod. 365. https://doi.org/10.1016/j.jclepro.2022.132755.

Gola, D., Kumar Tyagi, P., Arya, A., Chauhan, N., Agarwal, M., Singh, S.K., Gola, S., 2021. The impact of microplastics on marine environment: a review. Environ. Nanotechnol. Monit. Manag. https://doi.org/10.1016/j.enmm.2021.100552.

Guo, J.J., Huang, X.P., Xiang, L., Wang, Y.Z., Li, Y.W., Li, H., Cai, Q.Y., Mo, C.H., Wong, M.H., 2020. Source, migration and toxicology of microplastics in soil. Environ. Int. https://doi.org/10.1016/j.envint.2019.105263.

Hahn, M.W., O'Melia, C.R., 2004. Deposition and Reentrainment of Brownian particles in porous media under unfavorable chemical conditions: some concepts and applications. Environ. Sci. Technol. 38. https://doi.org/10.1021/es030416n.

Han, N., Zhao, Q., Ao, H., Hu, H., Wu, C., 2022. Horizontal transport of macro- and microplastics on soil surface by rainfall induced surface runoff as affected by vegetations. Sci. Total Environ. 831. https://doi.org/10.1016/j.scitotenv.2022.154989.

Hannun, J.A., Al-Raoush, R.I., Jarrar, Z.A., Alshibli, K.A., Jung, J., 2022. Fines effect on gas flow in sandy sediments using μCT and pore networks. J. Nat. Gas Sci. Eng. 108. https://doi.org/10.1016/j.jngse.2022.104834.

Harley-Nyang, D., Memon, F.A., Osorio Baquero, A., Galloway, T., 2023. Variation in microplastic concentration, characteristics and distribution in sewage sludge & biosolids around the world. Sci. Total Environ. 891. https://doi.org/10.1016/j.scitotenv.2023.164068.

He, H., Wu, T., Chen, Y.F., Yang, Z., 2023. A pore-scale investigation of microplastics migration and deposition during unsaturated flow in porous media. Sci. Total Environ. 858. https://doi.org/10.1016/j.scitotenv.2022.159934.

Heiss, J.W., Post, V.E.A., Laattoe, T., Russoniello, C.J., Michael, H.A., 2017. Physical controls on biogeochemical processes in intertidal zones of beach aquifers. Water Resour. Res. 53. https://doi.org/10.1002/2017WR021110.

Horton, A.A., Walton, A., Spurgeon, D.J., Lahive, E., Svendsen, C., 2017. Microplastics in freshwater and terrestrial environments: evaluating the current understanding to identify the knowledge gaps and future research priorities. Sci. Total Environ. https://doi.org/10.1016/j.scitotenv.2017.01.190.

Jacques, O., Prosser, R.S., 2021. A probabilistic risk assessment of microplastics in soil ecosystems. Sci. Total Environ. 757. https://doi.org/10.1016/j.scitotenv.2020.143987.

Jannesarahmadi, S., Aminzadeh, M., Raga, R., Shokri, N., 2023. Effects of microplastics on evaporation dynamics in porous media. Chemosphere 311. https://doi.org/10.1016/j.chemosphere.2022.137023.

Jarrar, Z.A., Al-Raoush, R.I., Hannun, J.A., Alshibli, K.A., Jung, J., 2020. 3D synchrotron computed tomography study on the influence of fines on gas driven fractures in Sandy Sediments. Geomech. Energy Environ. 23, 100105. https://doi.org/10.1016/j.gete.2018.11.001.

Jarrar, Z.A., Al-Raoush, R.I., Hannun, J.A., Alshibli, K.A., 2021. New model for estimating geometric tortuosity of variably saturated porous media using 3D synchrotron microcomputed tomography imaging. Soil Sci. Soc. Am. J. 85. https://doi.org/10.1002/saj2.20289.

Jiang, Y., Yin, X., Xi, X., Guan, D., Sun, H., Wang, N., 2021. Effect of surfactants on the transport of polyethylene and polypropylene microplastics in porous media. Water Res. 196. https://doi.org/10.1016/j.watres.2021.117016.

Jiang, Y., Zhou, S., Fei, J., Qin, Z., Yin, X., Sun, H., Sun, Y., 2022. Transport of different microplastics in porous media: effect of the adhesion of surfactants on microplastics. Water Res. 215. https://doi.org/10.1016/j.watres.2022.118262.

Jung, J., Shuang, Cao, C., Shin, Y.-H.H., Al-Raoush, R.I., Alshibli, K., Choi, J.-W.W., Cao, S.C., Shin, Y.-H.H., Al-Raoush, R.I., Alshibli, K., Choi, J.-W.W., 2018. A microfluidic pore model to study the migration of fine particles in single-phase and multi-phase flows in porous media. Microsyst. Technol. 24, 1071–1080. https://doi.org/10.1007/s00542-017-3462-1.

Katsumi, N., Kusube, T., Nagao, S., Okochi, H., 2021. Accumulation of microcapsules derived from coated fertilizer in paddy fields. Chemosphere 267. https://doi.org/10.1016/j.chemosphere.2020.129185.

Koutnik, V.S., Leonard, J., Alkidim, S., DePrima, F.J., Ravi, S., Hoek, E.M.V., Mohanty, S.K., 2021. Distribution of microplastics in soil and freshwater environments: global analysis and framework for transport modeling. Environ. Pollut. 274. https://doi.org/10.1016/j.envpol.2021.116552.

Koutnik, V.S., Leonard, J., Brar, J., Cao, S., Glasman, J.B., Cowger, W., Ravi, S., Mohanty, S.K., 2022. Transport of microplastics in stormwater treatment systems under freeze-thaw cycles: critical role of plastic density. Water Res. 222. https://doi.org/10.1016/j.watres.2022.118950.

Li, X.H., Xu, H.X., Sun, Y.Y., Wu, J.C., 2021. Review on the environmental behaviors of microplastics in porous media. Zhongguo Huanjing Kexue/China Environ. Sci. 41 (6), 2798–2811.

Li, H., Wang, S., Chen, X., Xie, L., Shao, B., Ma, Y., 2023a. CFD-DEM simulation of aggregation and growth behaviors of fluid-flow-driven migrating particle in porous media. Geoenergy Sci. Eng. 231. https://doi.org/10.1016/j.geoen.2023.212343.

Li, J., Zhu, B., Huang, B., Ma, J., Lu, C., Chi, G., Guo, W., Chen, X., 2023b. Vertical distribution and characteristics of soil microplastics under different land use patterns: a case study of Shouguang City, China. Sci. Total Environ. 903. https://doi.org/10.1016/j.scitotenv.2023.166154.

Li, F., Huang, D., Wang, G., Cheng, M., Chen, H., Zhou, W., Xiao, R., Li, R., Du, L., Xu, W., 2024. Microplastics/nanoplastics in porous media: key factors controlling their transport and retention behaviors. Sci. Total Environ. https://doi.org/10.1016/j.scitotenv.2024.171658.

Liang, Y., Bradford, S.A., Simunek, J., Vereecken, H., Klumpp, E., 2013. Sensitivity of the transport and retention of stabilized silver nanoparticles to physicochemical factors. Water Res. 47. https://doi.org/10.1016/j.watres.2013.02.025.

Liang, Y., Luo, Y., Shen, C., Bradford, S.A., 2022. Micro- and nanoplastics retention in porous media exhibits different dependence on grain surface roughness and clay coating with particle size. Water Res. 221. https://doi.org/10.1016/j.watres.2022.118717.

Ling, X., Yan, Z., Lu, G., 2022. Vertical transport and retention behavior of polystyrene nanoplastics in simulated hyporheic zone. Water Res. 219. https://doi.org/10.1016/j.watres.2022.118609.

Liu, Z., Qin, Q., Hu, Z., Yan, L., Ieong, U.I., Xu, Y., 2020. Adsorption of chlorophenols on polyethylene terephthalate microplastics from aqueous environments: kinetics, mechanisms and influencing factors. Environ. Pollut. 265. https://doi.org/10.1016/j.envpol.2020.114926.

Liu, Y., Li, S., Wang, L., Zhang, P., Liu, T., Li, X., 2024. Temperature fluctuation in soil alters the nanoplastic sensitivity in wheat. Sci. Total Environ. 929. https://doi.org/10.1016/j.scitotenv.2024.172626.

Molnar, I.L., O'Carroll, D.M., Gerhard, J.I., 2011. Impact of surfactant-induced wettability alterations on DNAPL invasion in quartz and iron oxide-coated sand systems. J. Contam. Hydrol. 119. https://doi.org/10.1016/j.jconhyd.2010.08.004.

Nishad, S., Al-Raoush, R.I., 2021. Colloid retention and mobilization mechanisms under different physicochemical conditions in porous media: a micromodel study. Powder Technol. 377, 163–173. https://doi.org/10.1016/j.powtec.2020.08.086.

Nishad, S., Al-Raoush, R.I., Alazaiza, M.Y.D., 2021. Release of colloids in saturated porous media under transient hydro-chemical conditions: a pore-scale study. Colloids Surf. A Physicochem. Eng. Asp. 614, 126188. https://doi.org/10.1016/j.colsurfa.2021.126188.

O'Connor, D., Pan, S., Shen, Z., Song, Y., Jin, Y., Wu, W.M., Hou, D., 2019. Microplastics undergo accelerated vertical migration in sand soil due to small size and wet-dry cycles. Environ. Pollut. 249. https://doi.org/10.1016/j.envpol.2019.03.092.

Pazmino, E., Trauscht, J., Johnson, W.P., 2014. Release of colloids from primary minimum contact under unfavorable conditions by perturbations in ionic strength and flow rate. Environ. Sci. Technol. 48. https://doi.org/10.1021/es502503y.

Qi, R., Jones, D.L., Li, Z., Liu, Q., Yan, C., 2020. Behavior of microplastics and plastic film residues in the soil environment: a critical review. Sci. Total Environ. https://doi.org/10.1016/j.scitotenv.2019.134722.

Røy, H., Jae, S.L., Jansen, S., De Beer, D., 2008. Tide-driven deep pore-water flow in intertidal sand flats. Limnol. Oceanogr. 53. https://doi.org/10.4319/lo.2008.53.4.1521.

Santos, I.R., Eyre, B.D., Huettel, M., 2012. The driving forces of porewater and groundwater flow in permeable coastal sediments: a review. Estuar. Coast. Shelf Sci. https://doi.org/10.1016/j.ecss.2011.10.024.

Shen, C., Li, B., Huang, Y., Jin, Y., 2007. Kinetics of coupled primary- and secondary-minimum deposition of colloids under unfavorable chemical conditions. Environ. Sci. Technol. 41. https://doi.org/10.1021/es070210c.

Shen, C., Lazouskaya, V., Zhang, H., Wang, F., Li, B., Jin, Y., Huang, Y., 2012. Theoretical and experimental investigation of detachment of colloids from rough collector surfaces. Colloids Surf. A Physicochem. Eng. Asp. 410. https://doi.org/10.1016/j.colsurfa.2012.06.025.

Smith, M., Love, D.C., Rochman, C.M., Neff, R.A., 2018. Microplastics in seafood and the implications for human health. Curr. Environ. Health Rep. https://doi.org/10.1007/s40572-018-0206-z.

Song, W., Kovscek, A.R., 2016. Direct visualization of pore-scale fines migration and formation damage during low-salinity waterflooding. J. Nat. Gas Sci. Eng. 34, 1276–1283. https://doi.org/10.1016/j.jngse.2016.07.055.

Sun, Y., Gao, B., Bradford, S.A., Wu, L., Chen, H., Shi, X., Wu, J., 2015. Transport, retention, and size perturbation of graphene oxide in saturated porous media: effects of input concentration and grain size. Water Res. 68. https://doi.org/10.1016/j.watres.2014.09.025.

Sun, H., Zhou, S., Jiang, Y., Qin, Z., Fei, J., Sun, Y., Wang, J., Yin, X., 2022. Effect of cationic, anionic and non-ionic surfactants on transport of microplastics: role of adhesion of surfactants on the polyethylene surface. J. Hydrol. (Amst.) 612. https://doi.org/10.1016/j.jhydrol.2022.128051.

Tong, M., He, L., Rong, H., Li, M., Kim, H., 2020. Transport behaviors of plastic particles in saturated quartz sand without and with biochar/Fe_3O_4-biochar amendment. Water Res. 169. https://doi.org/10.1016/j.watres.2019.115284.

Torkzaban, S., Bradford, S.A., Wan, J., Tokunaga, T., Masoudih, A., 2013. Release of quantum dot nanoparticles in porous media: role of cation exchange and aging time. Environ. Sci. Technol. 47. https://doi.org/10.1021/es402075f.

Torkzaban, S., Bradford, S.A., Vanderzalm, J.L., Patterson, B.M., Harris, B., Prommer, H., 2015. Colloid release and clogging in porous media: effects of solution ionic strength and flow velocity. J. Contam. Hydrol. 181, 161–171. https://doi.org/10.1016/j.jconhyd.2015.06.005.

Tosco, T., Tiraferri, A., Sethi, R., 2009. Ionic strength dependent transport of microparticles in saturated porous media: modeling mobilization and immobilization phenomena under transient chemical conditions. Environ. Sci. Technol. 43. https://doi.org/10.1021/es900245d.

Wang, Q., Hernández-Crespo, C., Du, B., Van Hulle, S.W.H., Rousseau, D.P.L., 2021. Fate and removal of microplastics in unplanted lab-scale vertical flow constructed wetlands. Sci. Total Environ. 778. https://doi.org/10.1016/j.scitotenv.2021.146152.

Wang, X., Diao, Y., Dan, Y., Liu, F., Wang, H., Sang, W., Zhang, Y., 2022a. Effects of solution chemistry and humic acid on transport and deposition of aged microplastics in unsaturated porous media. Chemosphere 309. https://doi.org/10.1016/j.chemosphere.2022.136658.

Wang, Y., Xu, L., Chen, H., Zhang, M., 2022b. Retention and transport behavior of microplastic particles in water-saturated porous media. Sci. Total Environ. 808. https://doi.org/10.1016/j.scitotenv.2021.152154.

Wang, J., Guo, X., Brahney, J., Xu, Z., Hu, Y., Sheng, W., Chen, Y., Li, M., Guo, W., 2023. Growth of grasses and forbs, nutrient concentration, and microbial activity in soil treated with microbeads. Environ. Pollut. 324. https://doi.org/10.1016/j.envpol.2023.121326.

Xia, Y., Zhou, J.J., Gong, Y.Y., Li, Z.J., Zeng, E.Y., 2020. Strong influence of surfactants on virgin hydrophobic microplastics adsorbing ionic organic pollutants. Environ. Pollut. 265. https://doi.org/10.1016/j.envpol.2020.115061.

Xu, L., Liang, Y., Liao, C., Xie, T., Zhang, H., Liu, X., Lu, Z., Wang, D., 2022. Cotransport of micro- and nano-plastics with chlortetracycline hydrochloride in saturated porous media: effects of physicochemical heterogeneities and ionic strength. Water Res. 209. https://doi.org/10.1016/j.watres.2021.117886.

Yang, L., Zhang, Y., Kang, S., Wang, Z., Wu, C., 2021. Microplastics in soil: a review on methods, occurrence, sources, and potential risk. Sci. Total Environ. https://doi.org/10.1016/j.scitotenv.2021.146546.

Zhang, Y., Hubbard, S., Finsterle, S., 2011. Factors governing sustainable groundwater pumping near a river. Ground Water 49. https://doi.org/10.1111/j.1745-6584.2010.00743.x.

Zhang, Q., Hassanizadeh, S.M., Liu, B., Schijven, J.F., Karadimitriou, N.K., 2014. Effect of hydrophobicity on colloid transport during two-phase flow in a micromodel. Water Resour. Res. 50, 7677–7691. https://doi.org/10.1002/2013wr015198.

Zhao, B., Liu, Q., Santamarina, J.C., 2019. Particle migration and clogging in radial flow: a microfluidics study. In: Trends in Mathematics. https://doi.org/10.1007/978-3-319-99474-1_41.

Zhao, W., Su, Z., Geng, T., Zhao, Y., Tian, Y., Zhao, P., 2022. Effects of ionic strength and particle size on transport of microplastic and humic acid in porous media. Chemosphere 309. https://doi.org/10.1016/j.chemosphere.2022.136593.

Zhou, J., Xiong, J., Xie, X., Liu, Y., 2023. Clogging mechanism of bioretention cell with fine-grained soil medium. J. Water Process Eng. 53. https://doi.org/10.1016/j.jwpe.2023.103630.